Thru-Hole Epitaxy: A Highway for Controllable and Transferable Epitaxial Growth

Dongsoo Jang, Chulwoo Ahn, Youngjun Lee, Seungjun Lee, Hyunkyu Lee, Donghoi Kim, Yongsun Kim, Ji-Yong Park, Young-Kyun Kwon,* Jaewu Choi,* and Chinkyo Kim*

Controllable growth and facile transferability of a crystalline film with desired characteristics, acquired by tuning composition and crystallographic orientation, become highly demanded for advanced flexible devices. Here the desired crystallographic orientations and facile transferability of a crystalline film can be achieved by "thru-hole epitaxy" in a straightforward and undemanding manner with no limitation on the layer number and polarity of a 2D space layer and the surface characteristics. The crystallographic alignment can be established by the connectedness of the grown material to the substrate through a small net cross-sectional area of thru-holes, which also allows the straightforward detachment of the grown material. Thru-hole epitaxy can be adopted for the realization of advanced flexible devices on large scale with desired crystallographic orientation and facile transferability.

1. Introduction

It is a golden rule that epitaxial growth of a crystalline film is allowed only by direct bonding to a crystalline substrate. Recently, however, such a golden rule seems to be rebuffed by two epitaxial growth methods, van der Waals epitaxy (vdWE)[1–4] and remote epitaxy (RE).[5–7] It was claimed that these epitaxy methods enable one to grow crystalline domains on a 2D van der Waals overlayer without direct bonding to an underlying substrate. Another attention has been paid to these methods due to their exceptional benefit that grown crystalline films can be easily transferred to target substances or devices thanks to the weak physical interaction between the grown films and the 2D overlayer.[1,3,8–12] The main distinction between the two epitaxy methods is the crystallographic alignment of the grown domains whether with the 2D overlayer in vdWE or with the underlying substrate in RE. Despite their beneficial advantage of facile transferability, they have not been widely adopted for epitaxial growth because of the strictly stringent growth conditions they require. They need not only an extremely high quality of 2D crystalline van der Waals layer but also at most one or two layers of nonpolar 2D overlayer on a strong ionic or polar substrate (specifically for RE) or special nucleation sites (specifically for vdWE).

Here we present our epitaxy method called "thru-hole epitaxy" (THE), which allows us to controllably grow films crystallographically aligned with an underlying substrate and to readily detach them from the substrate without any strictly stringent conditions required by vdWE and RE. Our THE is composed of two processes through nanoscale thru-holes sparsely distributed in the space layer: nucleation on the exposed substrate and lateral growth over the space layer.[13,14] Thru-hole epitaxy is similar to epitaxial lateral overgrowth, in which the nucleation occurs on the small exposed areas of the substrate and then lateral growth proceeds over the mask layer of SiO_2. However, in thru-hole epitaxy, the detachment of the grown film from the substrate can be readily done by using a thermal release tape due to both the small number and net cross-sectional area of thru-holes after either a few or multiple stacking of 2D materials. This readily detachable feature of the materials grown by thru-hole epitaxy makes thru-hole epitaxy essentially different from conventional epitaxial lateral overgrowth. Moreover, that feature is also associated with the advantage of using h-BN instead of SiO_2 as the mask layer for thru-hole epitaxy because there is only a weak van der Waals interaction between 2D masks material and the material grown over it.

In comparison with thru-hole epitaxy, quasi van der Waals epitaxy[15–18] does not require the connectedness between the grown material and the underlying substrate. Instead, the single crystallinity of the grown material comes from the single crystallinity of 2D layers. In other words, the difference

D. Jang, Y. Lee, S. Lee, Y.-K. Kwon, C. Kim
Department of Physics
Kyung Hee University
Seoul 02447, Korea
E-mail: ykkwon@khu.ac.kr; ckim@khu.ac.kr
C. Ahn, H. Lee, D. Kim, Y.-K. Kwon, J. Choi, C. Kim
Department of Information Display
Kyung Hee University
Seoul 02447, Korea
E-mail: jaewuchoi@khu.ac.kr
Y. Kim, J.-Y. Park
Department of Physics and Department of Energy Systems Research
Ajou University
Suwon 16499, Korea

The ORCID identification number(s) for the author(s) of this article can be found under https://doi.org/10.1002/admi.202201406.

between thru-hole epitaxy and quasi van der Waals epitaxy is associated with where the crystallinity of the grown material comes from: either from the single crystalline substrate (thru-hole epitaxy) or single crystalline 2D layer (quasi van der Waals epitaxy). Thus, the advantage of thru-hole epitaxy over quasi van der Waals epitaxy is that no single crystalline 2D layers are required to grow a single crystalline material on top of the 2D layers as long as the underlying substrate is single crystalline and the connectedness is established between the substrate and the grown material through thru-holes.

As a demonstration of our THE, we grew epitaxial GaN domains, which are crystallographically aligned respectively to sapphire substrates with three different surface orientations and can be easily detached by a thermal release tape, under various et mediocri conditions. Our THE employed by these advantages can be a promising method for advancing flexible and large-scale electronics and optoelectronics. Furthermore, we suggest that our THE be a universal platform to explain various epitaxy methods in terms of the distribution of thru-holes.

2. Results and Discussion

To grow crystalline domains which can be easily detachable and to utilize them for flexible device application, we originally aimed at growing GaN domains by using vdWE on a thick and polycrystalline h-BN space layer (see Figure S1, Supporting Information) transferred onto a substrate. The thickness of h-BN transferred once is estimated to be about 3 nm. In hydride vapor phase epitaxy, the decomposition of NH_3 provides nitrogen species, and HCl flown over metal Ga produces GaCl, the decomposition of which provides Ga species to the substrate. The typical flow rates of NH_3 and HCl were 1500 and 10 sccm, respectively. The growth temperature was 960°C. To our surprise, however, we observed what we

had never expected: readily transferable GaN domains crystallographically aligned not with h-BN but with any underlying substrates used.

2.1. Seemingly Beyond Remote Epitaxy

To achieve our original goal, we grew GaN domains on a thick and polycrystalline h-BN space layer transferred onto r-sapphire substrates. The thickness of h-BN was deliberately chosen by multiple transfers (see Experimental Section) with an intention to make the influence of a substrate completely negligible. In contrary to our expectation, it was observed that those GaN domains grown on a h-BN/r-sapphire substrate exhibit a gable-roof-shape, indicating [11$\bar{2}$0]-orientation, as if directly grown on the bare r-sapphire substrate,[19–21] as shown in a secondary electron image (SEI) of **Figure 1**a and Figure S2, Supporting Information, regardless of the number of transfer times. Even more surprisingly, those [11$\bar{2}$0]-oriented gable-roof-shaped GaN domains were all in-plane aligned with one another on the polycrystalline thick h-BN layer, clearly indicating that the growth result is not what is expected in vdWE but under either the direct or teleported influence of the underlying substrate. The crystallographic alignment of those GaN domains with the r-sapphire substrate is confirmed by X-ray diffraction (XRD) measurement as shown in Figure 1b,c.

Not just on an r-sapphire substrate, similar results were observed on h-BN/c- and m-sapphire substrates as shown in Figure S3a–c,d–f, Supporting Information, respectively. XRD θ–2θ- and ϕ-scan data reveal that the orientation of GaN grown on h-BN/c-sapphire is [0002] whereas that on h-BN/m-sapphire is [1$\bar{1}$00], [1$\bar{1}$03], and [11$\bar{2}$2]. The observed orientation is exactly the same as the preferred orientation of GaN grown on bare c- and m-oriented sapphire substrates[22–30] verified by $\Delta\phi_{c1} = \Delta\phi_{c2} = \Delta\phi_{c3} = \Delta\phi_{c4} = \Delta\phi_{c5} = 60°$, $\Delta\phi_{c6} = 30°$, $\Delta\phi_{m1} = 261°$, $\Delta\phi_{m2} = 10°$,
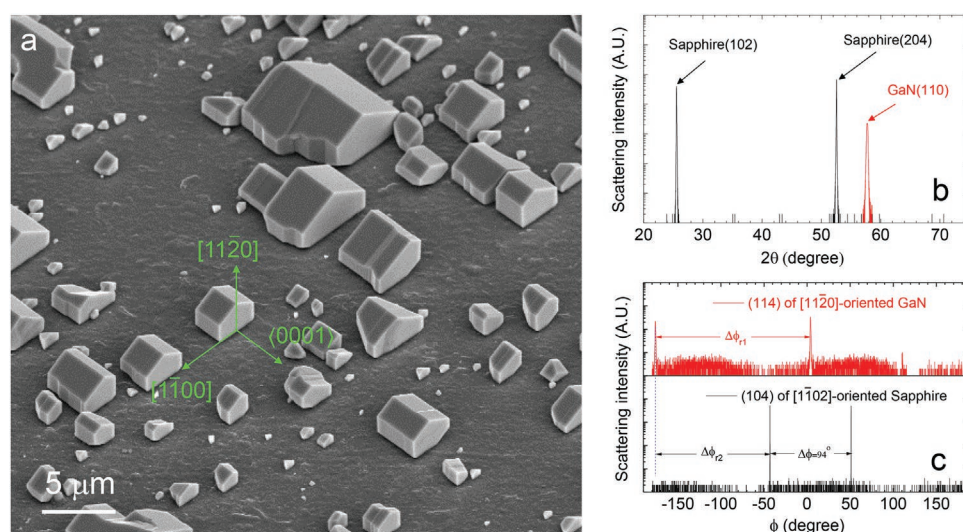

Figure 1. Crystallographic alignment of GaN domains grown on h-BN/r-sapphire verified by SEI and XRD. a) An SEI of typical GaN domains grown on h-BN transferred eight times onto r-sapphire. The gable-roof-shaped GaN domains are aligned in parallel and their crystallographic orientations are labeled. X-ray scattering intensity of GaN and r-sapphire in b) θ–2θ and c) ϕ scan. The observed [11$\bar{2}$0]-oriented GaN domains are exactly aligned with r-sapphire as if they were grown on the bare r-sapphire substrate as indicated by $\Delta\phi_{r1} = 180°$ and $\Delta\phi_{r2} = 133°$.

**ADVANCED
SCIENCE NEWS**

www.advancedsciencenews.com

**ADVANCED
MATERIALS
INTERFACES**

www.advmatinterfaces.de

$\Delta\phi_{m3} = 180°$, $\Delta\phi_{m4} = 48°$, $\Delta\phi_{m5} = 79°$, $\Delta\phi_{m6} = 101°$, $\Delta\phi_{m7} = 79°$, and $\Delta\phi_{m8} = 8°$. We observed the exact one-to-one correspondence in Bragg peaks of GaN domains respectively grown on *h*-BN/sapphire and bare sapphire as illustrated in Figure S4, Supporting Information. It is clear that the crystallographic alignment of GaN domains was definitely determined by the underlying sapphire substrates. These results imply that this puzzling growth process would be applicable to any crystalline substrates because the crystallographic alignment of GaN was well established in all *r*-, *c*-, and *m*-oriented sapphire substrates. It seemed that we dramatically extended the applicable growth regime of the remote epitaxy, resulting from the crystallographic information of sapphire teleported to GaN even across a thick *h*-BN space layer. What caused this alignment possible only by the influence of an underlying substrate, even in the presence of a thick *h*-BN space layer in-between?

To answer this question, we extensively performed transmission electron microscopy (TEM) measurements. Figure S5a, Supporting Information, shows a cross-sectional TEM image across the interfacial region of GaN and *r*-sapphire with a thick *h*-BN space layer in-between, marked in the red dotted box shown in cross-sectional TEM image in Figure S6, Supporting Information. It shows that there appears to be no direct contact areas between GaN and sapphire. In fact, Figure S5b–c, Supporting Information, showing zoomed-in TEM images of two areas near the interface marked by dashed cyan and green boxes in Figure S5a, Supporting Information, still reveal no sign of direct contact with the underlying sapphire substrate. (The thickness of *h*-BN transferred once is estimated to be about ≈3 nm.) The fast Fourier transformation (FFT) analysis shown in Figure S5d–g, Supporting Information, revealed that GaN, which is [11$\bar{2}$0]-oriented, right above thick *h*-BN was aligned with *r*-sapphire consistent with XRD measurements shown in Figure 1b,c. As can be seen from the figures, no compelling evidence to answer the question raised was seen in these TEM images at first sight.

The answer to the question came serendipitously from much thorough analysis of TEM images of interfacial regions. **Figure 2**a shows a high-resolution cross-sectional TEM image revealing the interfacial region marked by the yellow dashed box in Figure S5a, Supporting Information. Intriguingly, GaN was directly connected to the *r*-sapphire substrate through thru-holes in *h*-BN in spite of multiple transfers of *h*-BN (Figure S7, Supporting Information). As shown in Figure 2b,c, FFTs near thru-holes through which GaN and sapphire are connected show the crystallographic alignment of GaN with underlying sapphire. These high-resolution TEM and FFTs unveiled that the origin of this striking crystallographic alignment of GaN is epitaxial growth through thru-holes in *h*-BN, which we called thru-hole epitaxy (THE). We would like to emphasize that holes do not need to be perfectly vertical at all to serve as thru-holes. As long as they can establish the connectedness between GaN and the underlying substrate, those holes can serve as thru-holes because the perfect verticalness is not the requirement for holes to serve as thru-holes. It can be naturally inferred that GaN nucleated on exposed sapphire through thru-holes must have laterally grown over a thick *h*-BN space layer as seen in Figure S5b, Supporting Information. Our experimental results,

absolutely unexpected by vdWE or RE, were made possible not because the remoteness was mysteriously enhanced but because the direct bonding between GaN and sapphire was securely established. In addition, we carried out time evolution experiments of GaN with growth time. As clearly seen in the optical microscopy images (Figure S8, Supporting Information), no additional nucleation of GaN domains was observed as the growth time increased while individual domains were grown laterally/vertically and merged. This result suggests that: 1) the nucleation was preferentially made at certain positions at which there are thru-holes; and 2) the 2D space layer served as the mask material for lateral overgrowth, not the additional nucleation sites as long as the density of thru-hole is large enough. Here we emphasize that there is no large area of thru-holes across the interface within each individual domain. In other words, the crystallographic alignment of a domain with the underlying substrate does not require a large area of thru-holes but only a small area, indicating that THE would perfectly fit for facile detachment of domains grown as shown below. It may be quite natural to ask a question about how such small holes in each stack can survive to become thru-holes even after multiple stacking. It can be easily guessed that holes in each stack can be much more likely to be connected with holes in the above- or below-stack if the holes in each stack are not isolated but connected. As a consequence, the probability of those holes in each stack can survive to become thru-holes in multi-stacked *h*-BN is quite increased in comparison with the case of isolated holes. In fact, our atomic force microscopy (AFM) topography of *h*-BN showed connected holes, which are in good agreement with the argument given above for the survival of thru-holes (see Figure S9, Supporting Information). The connected holes are highly related to the defective *h*-BN edges. Thus, the survival of thru-holes even after multiple stacking can be well understood.

The readily facile detachability of a grown film crystallographically aligned with an underlying substrate is considered to be the exclusive benefit of RE, which is only possible under stringent and ideal conditions. Our results shown above, however, suggest that THE can practically provide this benefit in an effortless manner. To check whether the grown film by THE is readily detachable as well, we carried out the detachability experiment. **Figure 3**a–c shows optical microscopy images of GaN domains looking dark (see Figure S10, Supporting Information) grown on *h*-BN/*r*-sapphire, *h*-BN/*r*-sapphire after GaN domains being removed by a thermal release tape, and detached GaN domains on a thermal release tape, respectively. Partially connected *a*-GaN domains were in the size of about 3.5 mm × 5.5 mm, and the crystallographic orientations of each domain were well aligned with one another. There were certain domains undetached, but most of the connected domains were well detached. These figures clearly show that GaN domains were readily detached simply by using a thermal release tape although they were connected to the substrate by thru-holes. These results suggest that THE can provide the aforementioned benefit in a straightforward manner by lifting any constraints on the number of layers, quality, and polarity of a 2D space layer imposed by RE. Furthermore, the AFM topography study on the *h*-BN/sapphire substrate after GaN detachment revealed spiky GaN stumps located within the thru-holes in *h*-BN (see Figure S11, Supporting Information). This result indicates that
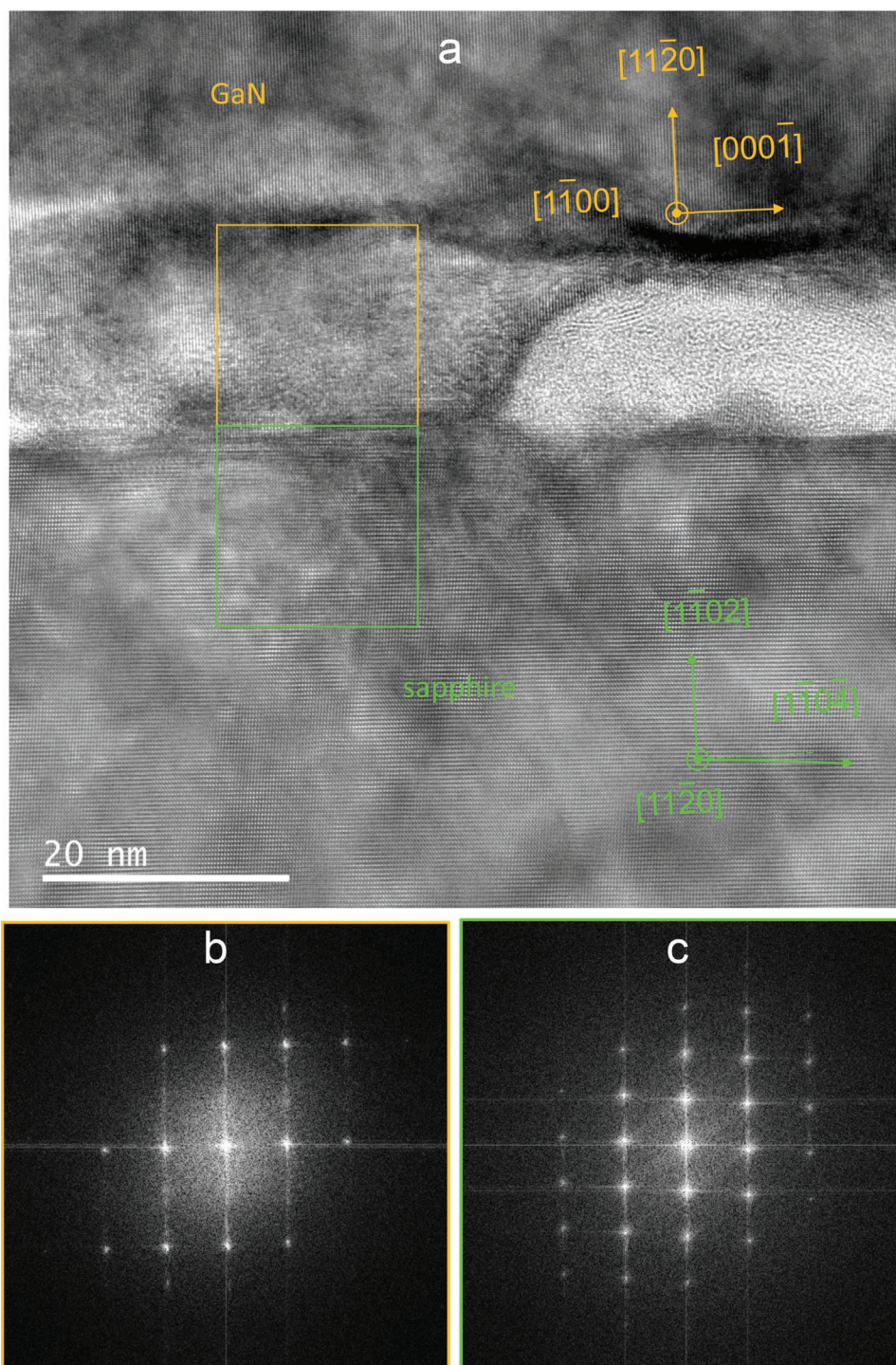
Figure 2. TEM and FFT verifying the connectedness. a) High-resolution cross-sectional TEM image, taken from the region enclosed by a yellow dashed box shown in Figure S5a, Supporting Information. GaN is seen to be grown directly on *r*-sapphire indicating the connectedness achieved, (Figure S7b, Supporting Information) and their crystallographic alignment is verified by FFTs in (b,c).

GaN is cut at the thinnest part, which is immersed in *h*-BN near the substrate, so that GaN stump was left after the detachment. This AFM topography once again confirmed that GaN was nucleated on sapphire through thru-holes in thru-hole epitaxy. It can be inferred from this image that the bottom surface of detached GaN would not be perfectly flat.

2.2. Extended Demonstration of THE

THE was found to be valid regardless of the thickness of a 2D layer containing thru-holes. We hypothesized that THE is still applicable to the system even with a much thicker 3D space layer as long as the connectedness and dominance over
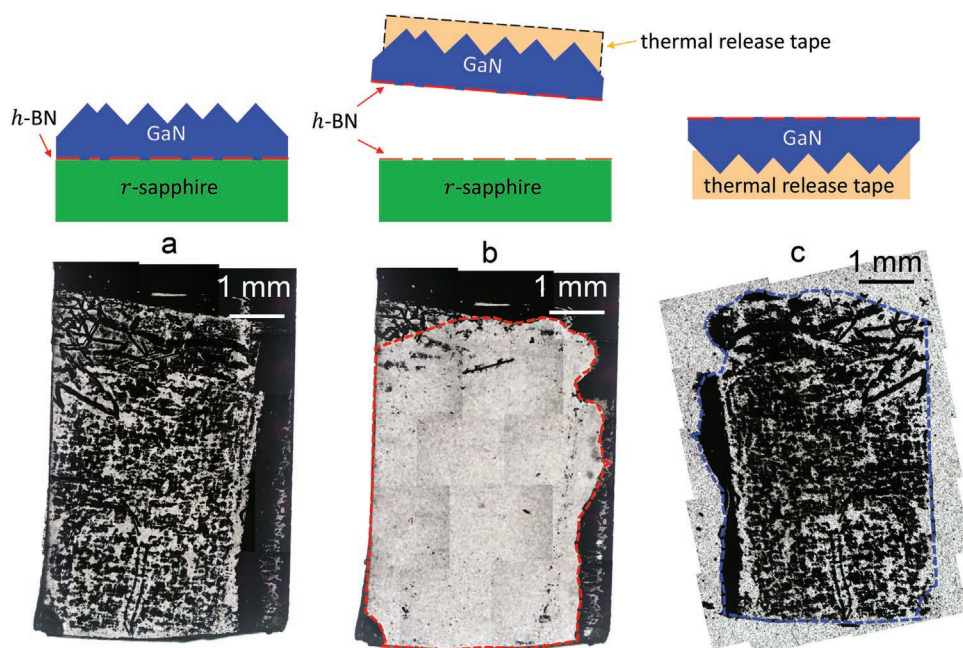
Figure 3. Facile detachment of GaN domains. Stitched optical microscopy images of a) as-grown GaN domains on six-time transferred *h*-BN space layer on an *r*-sapphire substrate, b) the *r*-sapphire substrate after GaN domains were detached by using a handy thermal release tape, and c) the detached GaN domains on the thermal release tape. Schematic diagrams corresponding to the samples shown in (a–c) are shown above each image. Although GaN is transparent, those GaN domains shown in the normally back-illuminated optical microscopy images in (a–c) look unusually dark due to their gable-roof shape as described in Figure S10, Supporting Information. The regions enclosed by the red and blue dashed lines represent the exposed *r*-sapphire and detached GaN. Note that there are dark-looking GaN domains with a gable-roof shape outside the region enclosed by the red dashed line indicating that they were directly grown on *r*-sapphire with the full connectedness since there is no *h*-BN space layer. The gable-roof shape of both detached and undetached GaN domains is another indication of the thru-hole epitaxy verifying the crystallographic alignments of GaN domains with the underlying sapphire substrate.

substrate-independent growth, are maintained. To verify our hypothesis, we introduced an additional 50-nm-thick SiO_2 space layer between *h*-BN and *r*-sapphire to form SiO_2/*r*-sapphire with *h*-BN overlayer. Subsequently, to achieve connectedness and dominance over substrate-independent growth, nanoscale thru-holes were produced in SiO_2 during the preheating step of the GaN growth by utilizing $FeCl_3$, which is known to thermally decompose SiO_2.[31] GaN domains grown in these experimental configurations were crystallographically aligned with *r*-sapphire as shown in **Figure 4**a–c, and thru-holes were confirmed in high-resolution TEM image as shown in Figure 4d. The number of thru-holes within an individual domain was very small as shown in Figure S12, Supporting Information, so that careful attention is required to spot thru-hole in TEM analysis. Once again, this suggests that the grown domains can be readily detachable. Moreover, we also successfully detached those [11$\bar{2}$0]-oriented GaN domains from *h*-BN/SiO_2/*r*-sapphire simply by using a thermal release tape as shown in **Figure 5**. Here we would like to emphasize that the crystallographic alignment is associated with the connectedness and dominance over substrate-independent growth, whereas *h*-BN or any 2D van der Waals space layer plays a role in not transferring the crystallographic information through but only in allowing the film grown above to be readily detachable. This result indicates that THE is robustly manifested even with a SiO_2 space layer as long as the connectedness and dominance over substrate-independent

growth are established by intentionally creating nanoscale thru-holes in SiO_2.

2.3. Readily Attainable Optimal Regimes for THE

We demonstrated that the crystallographic alignment and facile detachment are readily achieved by THE as long as connectedness and dominance over substrate-independent growth, both of which can be attainable in an effortless manner, are established. We now make a simple argument to discuss the conditions for connectedness and dominance over substrate-independent growth. The connectedness and dominance over substrate-independent growth are related to the size of a thru-hole, L, and areal number density, σ, of thru-holes, respectively. It should be noted that the crystallographic alignment depends on both the connectedness and dominance over substrate-independent growth, the latter of which has been often overlooked in situations where various growth types compete with one another. For the sake of simplicity, let us assume that every thru-hole is in a cylindrical shape and its areal number density is uniform. For the crystallographic alignment (CA), there are a critical size, L_c^{CA} and critical density, σ_c^{CA}. For $L > L_c^{CA}$, the domain grown from that thru-hole can be crystallographically aligned with an underlying substrate. For $\sigma < \sigma_c^{CA}$, additional domains with misaligned orientation may be grown on a 2D space layer between aligned domains even in the case of $L > L_c^{CA}$, so a film formed
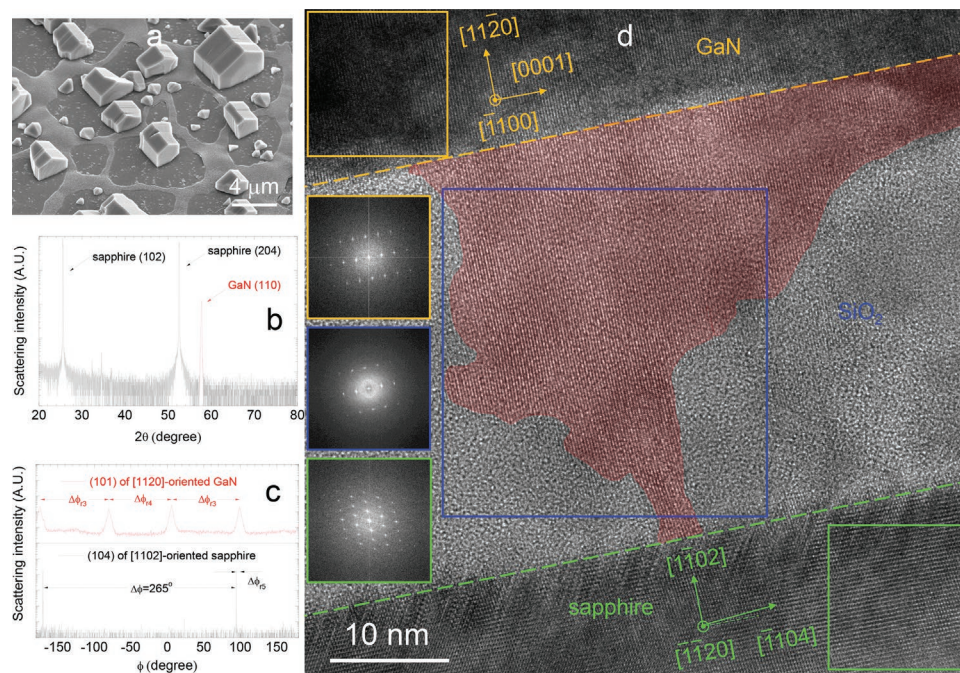
Figure 4. Compelling evidences of THE through a SiO$_2$ space layer. a) SEI of in-plane aligned GaN domains with gable-roof shape grown on h-BN/SiO$_2$/r-sapphire. X-ray scattering intensity of GaN and r-sapphire in b) θ–2θ and c) ϕ scan. Those [11$\bar{2}$0]-oriented GaN domains are still crystallographically aligned with r-sapphire in spite of 50-nm-thick SiO$_2$ space layer verified by $\Delta\phi_{r3} = 94°$, $\Delta\phi_{r4} = 86°$, and $\Delta\phi_{r5} = 5°$. d) High-resolution cross-sectional TEM image, taken from the region enclosed by a dashed red box in Figure S12a,b, Supporting Information, and FFTs for various regions. TEM and FFTs of the regions enclosed by the orange, blue, and green boxes confirm the connectedness by thru-hole epitaxy (shaded in red) and crystallographic alignment.

by merging individual domains is not crystallographically aligned but has mixed orientations. Note that L_c^{CA} and σ_c^{CA} are coupled with each other. It is of great importance that both L_c^{CA} and σ_c^{CA} depend on various factors such as the type of 2D space layer, a binding force between substrate and film materials, and even growth conditions. It should be noted that the same L and σ may or may not result in the crystallographic alignment of a given film material with a given 2D space layer and

substrate under distinct growth conditions because L_c^{CA} and σ_c^{CA} become different. For example, if the concentration of species arriving at the 2D mask material/substrate is increased, those species would form misaligned nuclei on the 2D mask material before they form aligned nuclei on the exposed substrate. In other words, σ_c would decrease in such a way that thru-hole epitaxy may fail even for the same σ at which thru-hole epitaxy would have been successful at a lower concentration of species
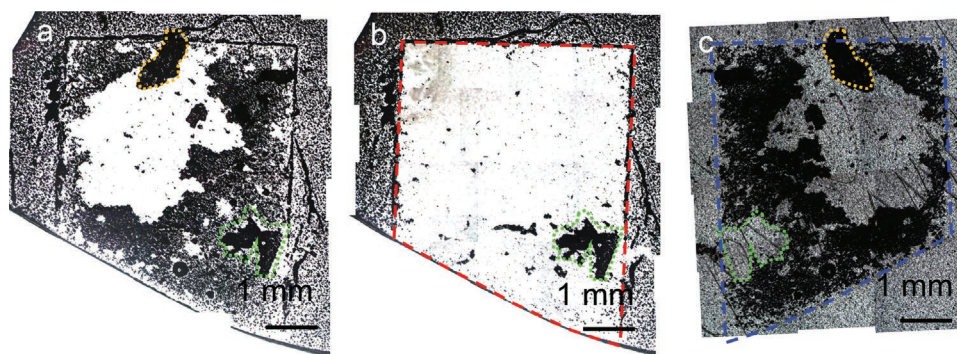

Figure 5. TRT transfer of GaN grown on h-BN/SiO$_2$/r-sapphire. Stitched optical microscopy images of a) as-grown GaN domains on a one-time transferred h-BN space layer on an SiO$_2$/r-sapphire substrate, b) the r-sapphire substrate after the GaN domains were detached by using a handy thermal release tape, and c) the detached GaN domains on the thermal release tape. As mentioned in Figure 3, the dark-looking GaN domains are all [11$\bar{2}$0]-oriented with the gable-roof shape. The white region in the middle of the sample in (a) is where GaN was self-separated during the cool-down process after the growth. The regions enclosed by the red and blue dashed lines represent the exposed r-sapphire and detached GaN. The regions enclosed by the green and yellow dotted lines represent the undetached and self-separated GaN domains. We speculate that this region enclosed by a green dashed line was not detached due to either the high connectedness or the direct bonding with SiO$_2$. Note that there are dark-looking GaN domains with a gable-roof shape outside the region enclosed by the red dashed line indicating that they were directly grown on SiO$_2$/r-sapphire without an h-BN space layer.

2201406 (6 of 12)

**ADVANCED
SCIENCE NEWS**

www.advancedsciencenews.com

**ADVANCED
MATERIALS
INTERFACES**

www.advmatinterfaces.de

arriving at the 2D mask material/substrate. Thus, $L > L_c^{CA}$ and $\sigma > \sigma_c^{CA}$ for the crystallographic alignment.

Likewise, the detachability is related to both size, L, and density, σ, of thru-holes. For the facile detachment (FD), there is a critical size, L_c^{FD}, and critical density, σ_c^{FD}. Thus, $L < L_c^{FD}$ and $\sigma < \sigma_c^{FD}$ for the facile detachment (Figure S13, Supporting Information). For successful detachment of crystallographically aligned film, $L_c^{CA} < L < L_c^{FD}$ and $\sigma_c^{CA} < \sigma < \sigma_c^{FD}$. The connectedness and dominance over substrate-independent growth can be controlled by adjusting the quality and thickness of a space layer (for example, the number of defects and the number of layers of h-BN or graphene). The better the quality of a 2D space layer the lower the density of thru-holes. Both crystallographic alignment and facile detachability can be achieved by THE, in principle, for any materials in quite a large subspace of growth parameter space. Schematic diagrams and a table summarizing the conditions for the optimal regime of THE are shown in Figure S14, Supporting Information. This is the biggest advantage of THE over other growth types. Our THE, as verified in our experimental results, is robust and dominant over other growth processes, indicating that our readily attainable growth conditions fall right in the optimal conditions for both connectedness and dominance over substrate-independent growth. Therefore, THE of crystallographically aligned GaN on h-BN/sapphire does not require the state-of-the-art perfection of h-BN at all.

It is quite reproducible to obtain a similar density of GaN domains in thru-hole epitaxy on h-BN transferred onto a sapphire substrate under the same experimental procedures. We have observed that the density of thru-holes varies depending on the growth settings of h-BN, but that holes are not likely to be completely eliminated. So, to some extent, holes in h-BN are universal although their density of them may vary. At this point, the surface preparation condition is not likely to be responsible for the formation of thru-holes, but we cannot pin down whether either growth or transfer or both is responsible for thru-holes.

The control of the uniformity of GaN grown by thru-hole epitaxy is highly desirable for advanced applications. However, this is beyond the present scope aiming at the concept proof of the THE. The uniformity control largely requires the manipulation of the density as well as the size of thru-holes formed in the 2D space layer. Once the uniformity is improved to some extent, the size of GaN grown by thru-hole epitaxy can be readily increased. This is presently investigated as the follow-up investigation.

2.4. Optimal Regime for THE with an Extremely Thin 2D Space Layer

We demonstrated the robustness of THE in the optimal conditions for both connectedness and dominance over substrate-independent growth with a thick 2D space layer. For the case in which the thickness of a 2D space layer is extremely thin (i.e., one monolayer), an additional growth process such as RE could be competitive. In this situation, it would be an interesting question to ask what would be the optimal regime for THE. It is not straightforward to answer this question, but it came to

our attention that the original proposers of RE tried to answer this question.[32]

In their experimental configuration,[32] they chose a nonionic material, Ge, to exclude RE. Then, they assumed that the existence of pinholes would result in THE, which was supposed to be a dominant growth type consequently resulting in a single crystalline film. In contrary to their assumption, the grown film was polycrystalline (Figure 4b,d,f of the paper in ref. [32]) so they excluded THE as a dominant growth mechanism over RE. Based on our description in the previous subsection, however, it seems that L and σ of their 2D space layer were below L_c^{CA} or σ_c^{CA} determined by their experimental configuration, simply indicating that the growth of domains with misaligned orientation was dominant over THE in that growth regime. If they had adjusted experimental configurations in such a way that either L and σ sufficiently increased or L_c^{CA} and σ_c^{CA} sufficiently decreased to satisfy $L > L_c^{CA}$ and $\sigma > \sigma_c^{CA}$, then THE would have occurred dominantly. We would like to emphasize that the existence of thru-holes does not necessarily guarantee THE as explained above. Therefore, it was irrelevant for them to exclude THE from the dominant mechanism over RE. In fact, we noticed another study in which the pin-hole-seeded lateral epitaxy of GaSb was observed with monolayer graphene as a 2D space layer.[14] This result can be interpreted from our description as the case in which the optimal regime for THE with an extremely thin 2D space layer was reached. If the density of pin-holes is reduced, RE would become initiated and begin to compete with pin-hole-based lateral epitaxy or THE, so that the optimal regime for THE is expected to be shifted with respect to that for THE determined when RE is unavailable. It is of great importance to reasonably estimate the optimal regime to determine whether either RE or THE is dominant. Despite our demonstration of the striking robustness and dominance of THE over other growth processes at a thick 2D space layer, no experimental evidence is currently available to estimate the optimal regime to determine the dominance of either THE or RE in a situation of an extremely thin 2D space layer with thru-holes. Thus, we have tried to carry out a computational simulation to explore such, but contrary to our purpose we came to encounter another conclusion that the validity of RE is questionable as follows.

2.5. Computational Evidence Questioning RE

The RE proposed by earlier studies[5–12] was validated mainly by the surface potential distribution calculated over a space layer complying with that of a substrate. We discussed some questions raised from the previous calculations in Note S1, Supporting Information. To verify whether such validation is indeed valid, we evaluated the electrostatic potential distributions on various surfaces including not only bare substrates such as sapphire, Si, GaAs, GaN, and LiF but also those substrates with a 2D graphene or h-BN overlayer, which will later be denoted as "overlayer/substrate," using the first-principles density functional theory (DFT) calculations. As an exemplary demonstration, we display the surface structures of the bare r-sapphire, graphene/r-sapphire, and h-BN/r-sapphire in the top view and their calculated surface potential profiles in
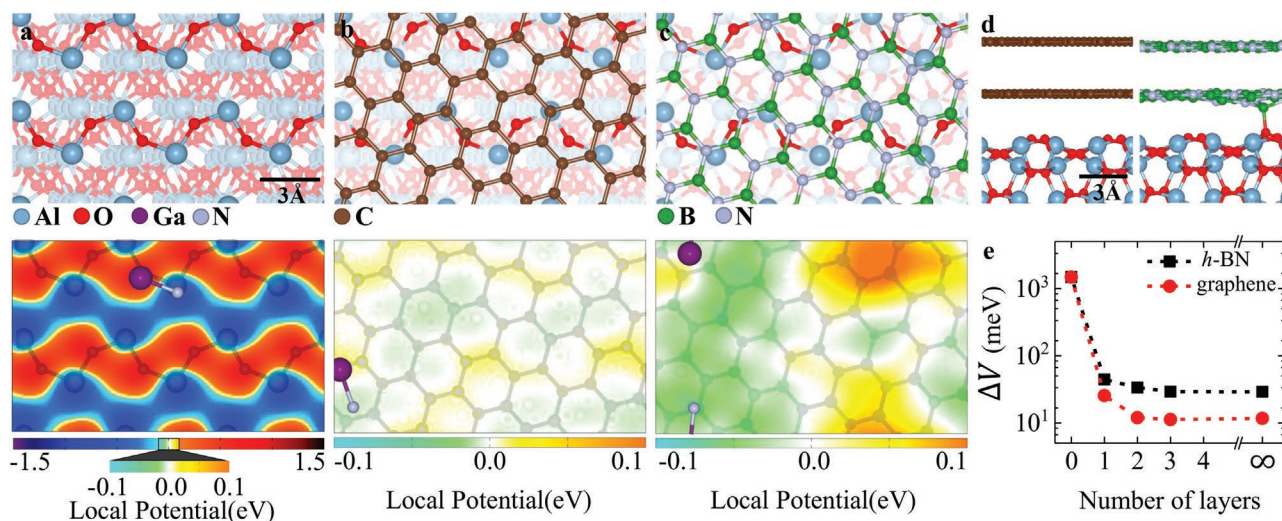
Figure 6. Structural configurations and surface potential profiles of sapphire with and without graphene or hBN overlayer. Structural configurations of a) bare r-sapphire, b) graphene, and c) h-BN monolayer on the r-sapphire, and their surface potential profiles evaluated at a distance d from the respective top surfaces. The distance d was chosen to be 2.0 and 3.0 Å on the bare r-sapphire and each of the overlayers, which are approximately bonding distances between GaN and the respective surfaces. d) Side views of bilayers of graphene and h-BN on the r-sapphire. e) The maximum potential differences ΔV observed between the Ga and N sites of a Ga–N dimer considered as an initial seed depicted in (a–c). The infinity indicates the 2D overlayer without the r-sapphire substrate. The topmost atomic layer overlaid on each color-coded potential profile is a guide for the eyes. The color bars indicate the potential variation relative to the average potential value set to be zero. Note that the potential variations on the overlayers were color-coded within a much narrower range. Each 2D space layer/r-sapphire is composed of a 2×3 supercell of the rectangular primitive unit cell of the r-sapphire and a $(\sqrt{13} \times \sqrt{13})R13.9°$ supercell of the rectangular $\sqrt{3}a \times a$ unit, where a is a lattice constant of the hexagonal primitive unit cell, cell of a 2D overlayer, which somewhat mimics a naturally-occurring incommensurate stacking.

Figure 6a–c, respectively. Here we emphasize that a computationally-convenient small commensurate stacking configuration introduced to resolve the lattice mismatch between the substrate and the 2D overlayer instigates an artificially periodic potential fluctuation, which would lead to a misinterpretation, as discussed later. To mimic a naturally-occurring incommensurate stacking, we thus constructed relatively a large supercell structure composed of 2D overlayer/r-sapphire.

As shown in the lower part of Figure 6a, the bare r-sapphire without a space layer generates a huge potential variation, which is attributed to both a strong ionic characteristic of Al–O bonds and an uneven surface configuration of the substrate. When a monolayer ($n = 1$) of the 2D space overlayer, either graphene or h-BN, covers the r-sapphire, not only is the surface potential variation drastically reduced due to the screening of the space layer, but it does not reflect the shape of the potential profile on the r-sapphire substrate, as shown in the lower parts of Figure 6b,c. With one more layer ($n = 2$) of the overlayer material, not to mention the complete dissimilarity between its surface potential distribution and that on the bare substrate, the surface potential variation becomes much smaller, being almost close to that over the overlayer itself without the substrate, since the second layer is essentially flat as shown in Figure 6d. Furthermore, the potential variations for $n \geq 3$ cases were found to be almost the same as that of either isolated graphene or h-BN, as shown in Figure S15, Supporting Information.

To examine whether the remote epitaxy would indeed have been eventuated on defect-free 2D space materials, we estimated the potential difference ΔV undergone by a Ga-N dimer regarded as a primordial growth seed that should anchor on

the 2D overlayer with a similar orientation to on the bare substrate to guarantee the remote epitaxy. Figure 6e shows ΔV as a function of the layer numbers n of 2D graphene and h-BN overlayers. Even with $n = 1$, ΔV was calculated to be only $\approx$1–2% of that on the bare sapphire, and rapidly converged to the value on the 2D overlayer without the substrate when $n \geq 2$. For comparison, over other substrates, such as Si, GaAs, GaN, and LiF, we evaluated their potential variations at $d = 3.0$ Å, near which the 2D space layer would locate, above their surfaces, to know over which substrate the potential variations emerge through a 2D space layer. As shown in Figure S16, Supporting Information, the magnitude of the evaluated potential variation only over the GaN substrate is similar to that over the r-sapphire, but those over the other substrates are much smaller. Thus, the teleportation of substrate potential variations through a 2D space layer is not likely to occur over any kind of substrates as seen in Figure 6 for r-sapphire. It is also noted that the shift of optimal regime for THE turns out to be negligibly small because ΔV's on 2D monolayer h-BN and graphene are almost similar to those values on their corresponding thick 2D layers. Figure 6e shows $\Delta V \lesssim 20$ meV on graphene and $\lesssim 50$ meV on h-BN, which is related to a maximum surface diffusion barrier. Of course, there will be various surface diffusion paths available, the real diffusion barrier would be even lower. In addition, the adsorption energy of adatoms is also an order of a few tens of meV due to the inert nature of graphene and h-BN, which are dangling-bond-free van der Waals 2D materials.[33–36] The growth temperature of epitaxial GaN is over 1230 K corresponding to over 100 meV, which is essentially the thermal energy of adatoms. Therefore, during the growth process at such temperatures, source particles would diffuse quite freely
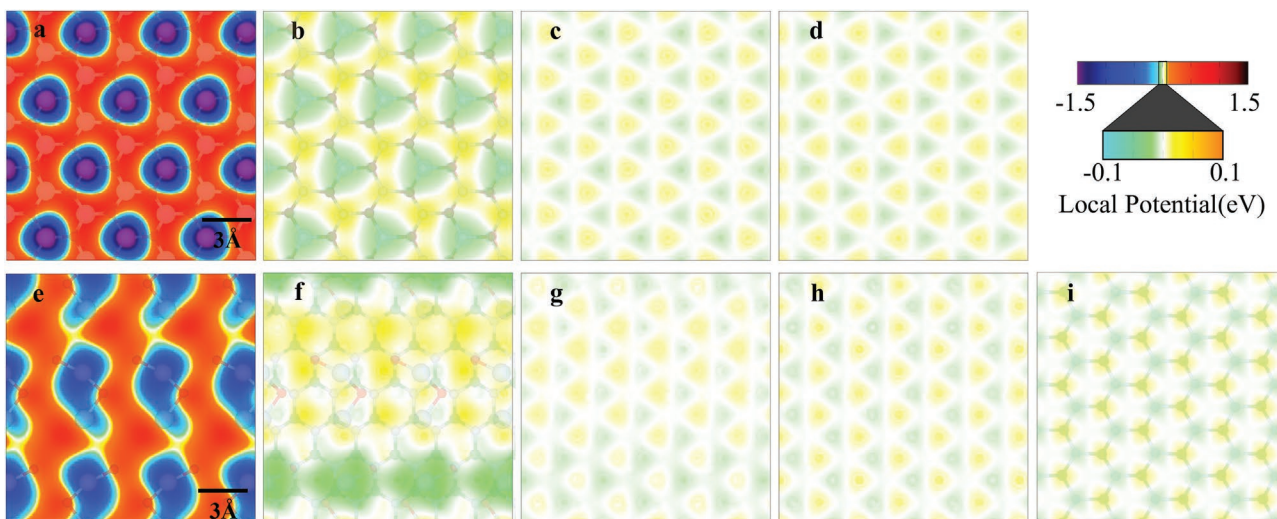
**ADVANCED
SCIENCE NEWS**

www.advancedsciencenews.com

**ADVANCED
MATERIALS
INTERFACES**

www.advmatinterfaces.de

Figure 7. Surface potential profiles of *h*-BN on *c*- and *m*-sapphire substrate. Surface potential profiles evaluated at a distance *d* from the respective top surfaces for a) bare *c*-sapphire, b) mono-, c) bi-, and d) tri-layer *h*-BN on *c*-sapphire, and e) bare *m*-sapphire, f) mono-, g) bi-, h) tri-, and i) hex-layer *h*-BN on *m*-sapphire, respectively. The distance *d* was chosen to be 2.0 Å on the bare *c*- and *m*-sapphire and 3.0 Å on each of the overlayers, which are approximately bonding distances between GaN and the respective surfaces. When the number of layers of *h*-BN is larger than one, the calculated potential profiles on both *c*- and *m*-sapphire are almost the same as that on the six layers of *h*-BN implying a negligibly small contribution of sapphire substrates. The color bars indicate the potential variation relative to the average potential value set to be zero. The potential variations on the *h*-BN overlayers were color-coded within a much narrower range. Note that the symmetry of potential variation, observed in (b), similar to that of bare *c*-sapphire is not actual but fictitious due to a lattice distortion caused by the choice of a supercell as described in Figure 8.

on these 2D materials rather than anchor at a certain site to form nucleates for epitaxial growth.

We further investigated the potential variations on the *c*- and *m*-sapphire substrates while increasing the layer number *n* of the *h*-BN space material from $n = 0$ to $n = 3$, whose trends are essentially identical to that on the *r*-sapphire case, as shown in **Figure 7**. To verify the effect of an artificially-generated periodicity caused by the strain applied to forcibly match the lattice mismatch between the substrate and the space layer as mentioned above, we evaluated the surface potential profiles over various stacking configurations of *h*-BN/*c*-sapphire, the combination of which clearly evinces such stacking effect. As displayed in **Figure 8**, the calculated potential variations are very sensitive to a choice of stacking configurations. Especially, in small supercell configurations, local potential variations look as if that of the substrate would be reflected over the 2D space layer, but this is a misleading artifact caused by such a forcibly matched stacking to make it commensurate. Therefore, the potential fluctuation of 2D material/substrate does not truly reflect the orientation and periodicity of the underlying substrate if the artifact originating from artificial stacking configurations is simply excluded. For a detailed explanation, see Note S2, Supporting Information. Based on our calculations, the remoteness of the RE[5–12] appears not to be fulfilled in general unless an exceptional condition, if any, would be accidentally realized.

Furthermore, we show that the features demonstrated by RE can also be explained by THE. These features are as follows: crystallographic alignment of a grown film with an underlying substrate, crystallographic alignment limited by layer number of 2D space material, ionicity dependence of crystallographic alignment, and easy detachability. A more detailed explanation is given in Supplementary Note S3, Supporting Information.

3. Conclusion

We have shown that thru-hole epitaxy through different types of thick space layers (e.g., polar *h*-BN or *h*-BN/SiO₂) is a surprisingly robust growth process to result in crystallographically aligned domains accompanied by a facile detachment under readily attainable conditions in a straightforward and undemanding manner. This growth behavior can provide the great advantage of detachable epitaxial film growth with no constraint on the state-of-the-art transfer perfection of 2D materials and the thickness of which should be less than a few layers imposed by the RE. Computational simulation suggests that the remoteness is not strong enough to fulfill RE, which has not been rigorously verified yet.

4. Experimental Section

Processes of the Thru-Hole Epitaxy: The thru-hole epitaxy consisted of the following processes, growth and transfer of *h*-BN, and growth of GaN, which were carried out with no special optimization. Despite no optimization, the thru-hole epitaxy was accomplished to the extent demanded, indicating that state-of-the-art perfection was not necessary for the thru-hole epitaxy.

Growth of h-BN: A polycrystalline *h*-BN thin film was grown on a Cu foil by chemical vapor deposition (CVD) at 1000 °C with hydrogen (50 sccm) and argon (100 sccm) as a carrier gas as shown in Figure S1, Supporting Information. Growth was carried out with ammonia borane (NH₃BH₃) as a precursor for 2 h after 2-h annealing of the Cu foil. The thickness of a multilayer *h*-BN transferred once was roughly estimated to be ≈3 nm by transmission electron microscopy. The chemical identification of *h*-BN is shown in Figure S7, Supporting Information.

Transfer of h-BN: This CVD-grown *h*-BN was transferred onto *r*-, *c*-, and *m*-sapphire substrates by applying a wet transfer method with poly (methyl methacrylate) (PMMA). PMMA was spin-coated over *h*-BN
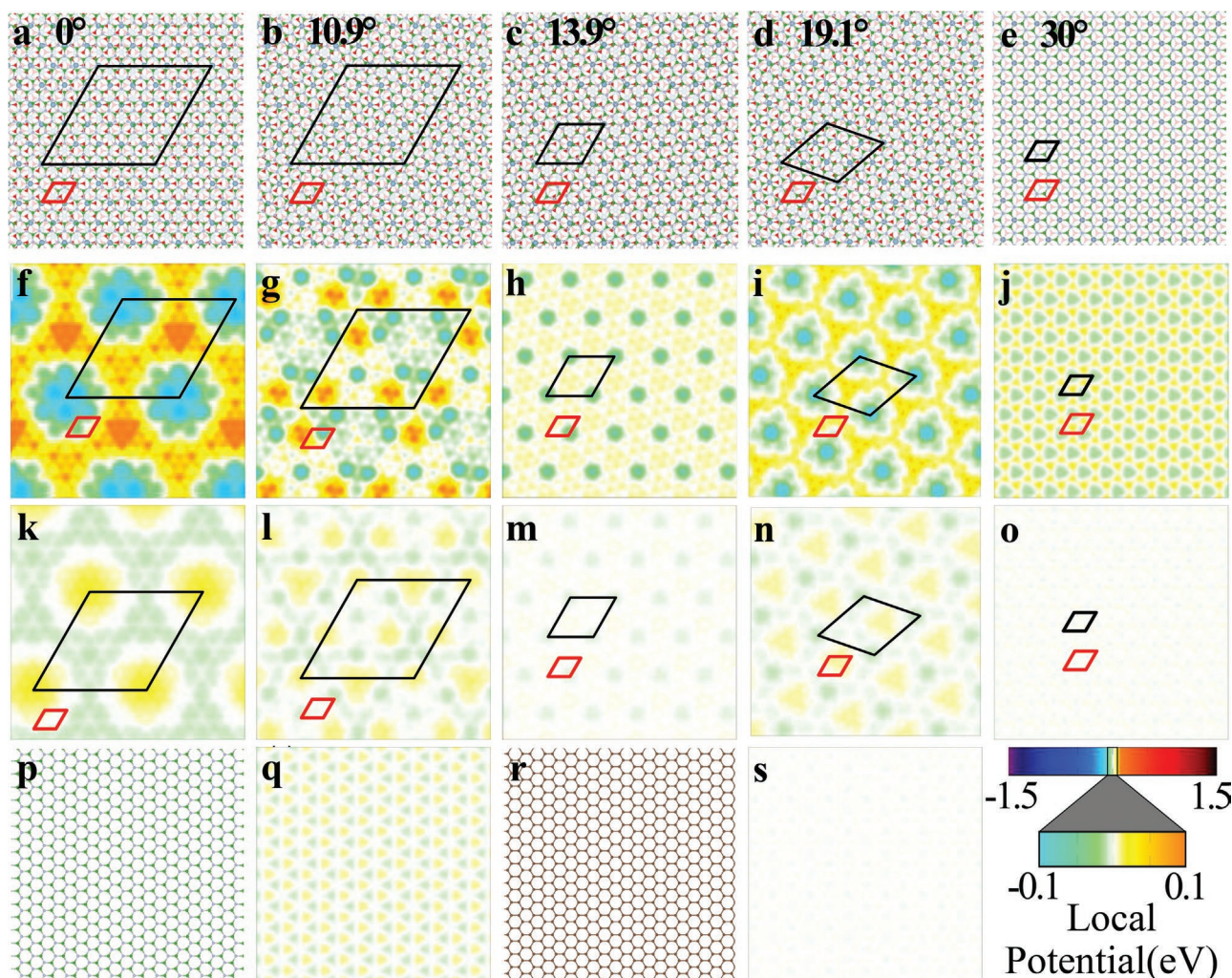
ADVANCED
SCIENCE NEWS
www.advancedsciencenews.com

ADVANCED
MATERIALS
INTERFACES
www.advmatinterfaces.de

Figure 8. Misleading artifacts caused by the choice of a supercell and the stacking configuration. a–e) Top views of relaxed structures for various configurations of *h*-BN/*c*-sapphire heterostructure. The numbers in degree indicate the angle between the *h*-BN zig-zag direction and the [10$\bar{1}$0] crystallographic direction of *c*-sapphire. f–j) Surface potential profiles calculated at *d* = 3.0 Å above the top surface of the structures shown in (a–e). k–o) Surface potential profiles calculated over the graphene, instead of *h*-BN, with the same configurations shown in (a–e). For comparison, over an isolated *h*-BN monolayer shown in (p), we also calculated its surface potential profile as shown in (q), as well as for an isolated graphene monolayer as shown in (r) and (s). The color bars indicate the potential variation relative to the average potential value set to be zero. The supercell of the combined 2D space layer and substrate is represented as a black parallelogram while a primitive unit cell of the underlying *c*-sapphire substrate is represented as a red parallelogram. It is clear that the surface potential profiles depend strongly on the stacking configuration as well as the supercell size, resulting in misleading artifacts, especially in small supercell configurations.

grown on a Cu foil, which was then etched with FeCl$_3$. PMMA/*h*-BN was transferred onto the desired substrate, and then that was rinsed twice with deionized water. After that, the PMMA was removed by acetone, and *h*-BN/substrate was cleaned by isopropyl alcohol. The extent of the connectedness and dominance over substrate-independent growth was intentionally controlled by changing the number of transfers made. For multiple transfers of *h*-BN, the transfer steps listed above were simply repeated.

Growth of GaN: GaN was grown on *h*-BN/sapphire or *h*-BN/SiO$_2$/sapphire by using hydride vapor phase epitaxy at 960 °C with HCl (10 sccm) flown over metal Ga and NH$_3$ (1500 sccm) carried by N$_2$.

Detachment of GaN: A TRT was applied onto the as-grown GaN domains. Then, the as-grwon GaN domains were detached from the *h*-BN/sapphire template by peeling off the TRT. The optical microscopy images of as-grown and detached GaN domains were taken using Olympus BX51M Metallurgical Microscope at the Multi Dimension Material Convergence Research Center of Kyung Hee University.

Electron Microscopy, Focused Ion Beam, and EDS: TEM and selected area diffraction measurements were performed by using a Thermo Fisher Titan 80-300 microscope operated at 300 kV. All the TEM images were taken in bright field mode. The available point resolution was better than 1 Å at the operating acceleration voltage. TEM images were recorded by using a charge-coupled camera (Gatan, Oneview095). Scanning TEM (STEM) and energy dispersive spectroscopy (EDS) analysis with Super-X EDS was made by using a Thermo Fisher Talos F200X at 200 kV with a probe size of ≈1 nm. SEIs were taken by using Hitachi S-4700. For the preparation of TEM samples, focused ion beam (Hitachi, NX5000) was utilized.

Computational Simulation: First-principles calculations were performed using the density functional theory[37] as implemented in Vienna ab initio simulation package (VASP).[38] The electronic wavefunctions were expanded by plane wave basis with a kinetic energy cutoff of 520 eV. The projector-augmented wave pseudopotentials[39,40] were employed to describe the valence electrons, and treated

exchange-correlation functional within the generalized gradient approximation of Perdew–Burke–Ernzerhof.[41] Interlayer interactions were incorporated with Grimme-D2 van der Waals correction.[42] To reduce long-range interactions from neighboring cells located along the out-of-plane or growth direction, a sufficiently large vacuum region of 20 Å was included. The Brillouin zone (BZ) of each structure was sampled using a separation of 0.04 Å^{-1} k-point mesh according to the Monkhost–Pack scheme.[43] The structures were relaxed until all forces became smaller than 0.02 eV Å^{-1}. The exchange-correlation potential was excluded in potential fluctuation maps because exchange-correlation potential on a long distance from the surface was incorrect within standard DFT.[6,44] Various 2D overlayer/sapphire supercell structures were constructed to avoid artificially generated periodic potentials.

Supporting Information

Supporting Information is available from the Wiley Online Library or from the author.

Conflict of Interest

The authors declare no conflict of interest.

Data Availability Statement

The data that support the findings of this study are available from the corresponding author upon reasonable request.

[1] H. Oh, Y. J. Hong, K.-S. Kim, S. Yoon, H. Baek, S.-H. Kang, Y.-K. Kwon, M. Kim, G.-C. Yi, *NPG Asia Mater.* **2014**, *6*, e145.

[2] D. Liang, T. Wei, J. Wang, J. Li, *Nano Energy* **2020**, *69*, 104463.

[3] F. Feng, X. Yang, Z. Zhang, D. Kang, J. Zhang, K. Liu, X. Li, J. Shen, F. Liu, T. Wang, P. Ji, F. Xu, N. Tang, T. Yu, X. Wang, D. Yu, W. Ge, B. Shen, *Adv. Funct. Mater.* **2019**, *29*, 1905056.

[4] M. De Luca, X. Cartoixà, J. Martín-Sánchez, M. López-Suárez, R. Trotta, R. Rurali, I. Zardo, *2D Mater.* **2020**, *7*, 025004.

[5] Y. Kim, S. S. Cruz, K. Lee, B. O. Alawode, C. Choi, Y. Song, J. M. Johnson, C. Heidelberger, W. Kong, S. Choi, K. Qiao, I. Almansouri, E. A. Fitzgerald, J. Kong, A. M. Kolpak, J. Hwang, J. Kim, *Nature* **2017**, *544*, 340.

[6] W. Kong, H. Li, K. Qiao, Y. Kim, K. Lee, Y. Nie, D. Lee, T. Osadchy, R. J. Molnar, D. K. Gaskill, R. L. Myers-Ward, K. M. Daniels, Y. Zhang, S. Sundram, Y. Yu, S.-H. Bae, S. Rajan, Y. Shao-Horn, K. Cho, A.Ougazzaden, J. C. Grossman, J. Kim, *Nat. Mater.* **2018**, *17*, 999.

[7] J. Jeong, Q. Wang, J. Cha, D. K. Jin, D. H. Shin, S. Kwon, B. K. Kang, J. H. Jang, W. S. Yang, Y. S. Choi, J. Yoo, J. K. Kim, C.-H. Lee, S. W. Lee, A. Zakhidov, S. Hong, M. J. Kim, Y. J. Hong, *Sci. Adv.* **2020**, *6*, eaaz5180.

[8] J. Jeong, K.-A. Min, D. H. Shin, W. S. Yang, J. Yoo, S. W. Lee, S. Hong, Y. J. Hong, *Nanoscale* **2018**, *10*, 22970.

[9] J. Jeong, K.-A. Min, B. K. Kang, D. H. Shin, J. Yoo, W. S. Yang, S. W. Lee, S. Hong, Y. J. Hong, *Appl. Phys. Lett.* **2018**, *113*, 233103.

[10] Y. Guo, X. Sun, J. Jiang, B. Wang, X. Chen, X. Yin, W. Qi, L. Gao, L. Zhang, Z. Lu, R. Jia, S. Pendse, Y. Hu, Z. Chen, E. Wertz, D. Gall, J. Feng, T.-M. Lu, J. Shi, *Nano Lett.* **2019**, *20*, 33.

[11] J. Jeong, D. K. Jin, J. Cha, B. K. Kang, Q. Wang, J. Choi, S. W. Lee, V. Y. Mikhailovskii, V. Neplokh, N. Amador-Mendez, M. Tchernycheva, W. S. Yang, J. Yoo, M. J. Kim, S. Hong, Y. J. Hong, *ACS Appl. Nano Mater.* **2020**, *3*, 8920.

[12] S.-H. Bae, H. Kum, W. Kong, Y. Kim, C. Choi, B. Lee, P. Lin, Y. Park, J. Kim, *Nat. Mater.* **2019**, *18*, 550.

[13] O. H. Nam, M. D. Bremser, T. S. Zheleva, R. F. Davis, *Appl. Phys. Lett.* **1997**, *71*, 2638.

[14] S. Manzo, P. J. Strohbeen, Z.-H. Lim, V. Saraswat, D. Du, S. Xu, N. Pokharel, L. J. Mawst, M. S. Arnold, J. K. Kawasaki, *Nat. Comm.* **2022**, *13*, 4014.

[15] F. Liu, Z. Zhang, X. Rong, Y. Yu, T. Wang, B. Sheng, J. Wei, S. Zhou, X. Yang, F. Xu, Z. Qin, Y. Zhang, K. Liu, B. Shen, X. Wang, *Adv. Funct. Mater.* **2020**, *30*, 2001283.

[16] Y. Song, Y. Gao, X. Liu, J. Ma, B. Chen, Q. Xie, X. Gao, L. Zheng, Y. Zhang, Q. Ding, K. Jia, L. Sun, W. Wang, Z. Liu, B. Liu, P. Gao, H. Peng, T. Wei, L. Lin, Z. Liu, *Adv. Mater.* **2022**, *34*, 2105851.

[17] F. Liu, T. Wang, Z. Zhang, T. Shen, X. Rong, B. Sheng, L. Yang, D. Li, J. Wei, S. Sheng, X. Li, Z. Chen, R. Tao, Y. Yuan, X. Yang, F. Xu, J. Zhang, K. Liu, X.-Z. Li, B. Shen, X. Wang, *Adv. Mater.* **2022**, *34*, 2106814.

[18] Z. Chen, Z. Liu, T. Wei, S. Yang, Z. Dou, Y. Wang, H. Ci, H. Chang, Y. Qi, J. Yan, J. Wang, Y. Zhang, P. Gao, J. Li, Z. Liu, *Adv. Mater.* **2019**, *31*, 1807345.

[19] D. Shin, S. Lee, M. Jue, W. Lee, S. Oh, C. Kim, *J. Appl. Cryst.* **2013**, *46*, 443.

[20] C. Chen, J. Zhang, J. Yang, V. Adivarahan, S. Rai, S. Wu, H. Wang, W. Sun, M. Su, Z. Gong, E. Kuokstis, M. Gaevski, M. A. Khan, *Jpn. J. Appl. Phys.* **2003**, *42*, L818.

[21] B. Imer, F. Wu, J. S. Speck, P. DenBaars, *J. Cryst. Growth* **2007**, *306*, 330.

[22] D. Kim, D. Jang, H. Lee, J. Kim, Y. Jang, S. Yoon, C. Kim, *Cryst. Growth Des.* **2020**, *20*, 6198.

[23] H. Lee, D. Jang, D. Kim, C. Kim, *J. Appl. Crystallogr.* **2019**, *52*, 532.

[24] H. Lee, D. Jang, D. Kim, H. S. Kim, C. Kim, *J. Mater. Chem. C* **2018**, *6*, 6264.

[25] P. Vennegues, T. Zhu, D. Martin, N. Grandjean, *J. Appl. Phys.* **2010**, *108*, 113521.

[26] Y. Seo, S. Lee, M. Jue, H. Yoon, C. Kim, *Appl. Phys. Exp.* **2012**, *5*, 121001.

[27] Y. Seo, S. Lee, M. Y. Ju, D. Shin, H. Park, C. Kim, *Cryst. Growth Des.* **2011**, *11*, 3930.

[28] Y. Seo, C. Kim, *Appl. Phys. Lett.* **2010**, *97*, 101902.

[29] H. Lee, M. Jue, H. Yoon, S. Lee, C. Kim, *Appl. Phys. Lett.* **2014**, *104*, 182105.

[30] M. Jue, C.-W. Kim, S.-H. Kang, H. Yoon, D. Jang, Y.-K. Kwon, C. Kim, *Sci. Rep.* **2015**, *5*, 16236.

[31] D. Jang, M. Jue, H. Yoon, C. Kim, *Curr. Appl. Phys.* **2016**, *16*, 93.

[32] H. Kim, K. Lu, Y. Liu, H. S. Kum, K. S. Kim, K. Qiao, S.-H. Bae, S. Lee, Y. J. Ji, K. H. Kim, H. Paik, S. Xie, H. Shin, C. Choi, J. H. Lee, C. Dong, J. A. Robinson, J.-H. Lee, J.-H. Ahn, G. Y. Yeom, D. G. Schlom, J. Kim, *ACS Nano* **2021**, *15*, 10587.

[33] S.-H. Jhi, Y.-K. Kwon, *Phys. Rev. B* **2005**, *71*, 035408.

[34] H. J. Song, Y. Lee, T. Jiang, A.-G. Kussow, M. Lee, S. Hong, Y.-K. Kwon, H. C. Choi, *J. Phys. Chem. C* **2008**, *112*, 629.

[35] Y.-K. Kwon, *J. Korean Phys. Soc.* **2010**, *57*, 778.

[36] Y. Lee, D.-G. Kwon, G. Kim, Y.-K. Kwon, *Phys. Chem. Chem. Phys.* **2017**, *19*, 8076.

[37] W. Kohn, L. J. Sham, *Phys. Rev.* **1965**, *140*, A1133.

[38] G. Kresse, J. Furthmüller, *Phys. Rev. B* **1996**, *54*, 11169.

[39] P. E. Blöchl, *Phys. Rev. B* **1994**, *50*, 17953.

[40] G. Kresse, D. Joubert, *Phys. Rev. B* **1999**, *59*, 1758.

[41] J. P. Perdew, K. Burke, M. Ernzerhof, *Phys. Rev. Lett.* **1996**, *77*, 3865.

[42] S. Grimme, *J. Comput. Chem.* **2006**, *27*, 1787.

[43] H. J. Monkhorst, J. D. Pack, *Phys. Rev. B* **1976**, *13*, 5188.

[44] Q. Wu, W. Yang, *J. Chem. Phys.* **2003**, *118*, 2498.